Axial-vector-coupling contribution to toponium resonances

PHYSICAL REVIEW D VOLUME 47, NUMBER 1 1 JANUARY 1993

Axial-vector-coupling contribution to toponium resonances

H. Murayama
Department of Physics, Tohoku University, Sendai, 980 Japan

Y. Sumino
Department of Physics, University of Tokyo, Tokyo, 113 Japan
(Received 20 May 1992)

We study the effect of $t\bar{t}Z$ axial-vector coupling to the $t\bar{t}$ pair production process near threshold at e^+e^- colliders. P-wave resonance states produced via axial-vector coupling interfere with S-wave resonance states due to the large top-quark width. This interference gives rise to the forward-backward asymmetry below threshold which grows from 0 to $\sim 7\%$ as m_t is increased from 100 to 200 GeV. Its α_s dependence is magnified simultaneously. The measurement of the forward-backward asymmetry may allow an efficient determination of α_s for a relatively heavy top quark.

PACS number(s): 13.65.+i, 13.20.Gd, 14.40.Gx

I. INTRODUCTION

It was first pointed out by Fadin and Khoze [1] that the $t\bar{t}$ threshold region at e^+e^- colliders provides a fairly clean test of perturbative QCD due to the large width of the top quark. The top-quark width grows rapidly as m_t increases [2], and the dominant decay modes of toponium resonances are expected to be almost saturated by the electroweak decay process of each constituent. This large width would act as an infrared cutoff, and hence we will be free from the theoretical uncertainties of low-energy QCD processes.

A quantitative analysis of the total cross sections in the $t\bar{t}$ threshold region was first performed in Ref. [1], and later refined in Ref. [3], where the Coulomb singularities were summed using the Green's function method. Recently, the authors of Ref. [4] made a quantitative analysis including the effect of the considerable reduction of the resonance widths below threshold, in which the importance of simultaneous measurements of the total and differential cross sections is stressed in order to determine α_s and m_t at a high precision near $t\bar{t}$ threshold, namely, $\Delta m_t < 1$ GeV.

To provide reliable theoretical predictions of the total and differential cross sections in the threshold region, it is desirable to include next-to-leading-order corrections to the cross sections. Some of them are already included in the above analyses. The leading-order terms at the threshold are identified with the Coulomb singularities (threshold singularities), where all the orders $(\alpha_s/\beta)^n$ are summed up [5, 6], with $\beta \simeq |\mathbf{p}_t|/m_t$. The next-to-leading-order corrections are the terms α_s^{n+1}/β^n, which can be regarded as the order α_s, or equivalently, order β corrections to the leading-order terms, since $\alpha_s^{n+1}/\beta^n = \alpha_s(\alpha_s/\beta)^n = \beta(\alpha_s/\beta)^{n+1}$. Thus, the next-to-leading-order corrections are expected to give order 10% corrections to the cross sections, and it is important to establish the full theoretical prediction to this order with regard to the future experiments. Further corrections from the terms $\sim \alpha_s^{n+2}/\beta^n$ are only of order 1%, which can be safely neglected for practical purposes. Summation over all these next-to-leading-order corrections is now underway [7].

Among these corrections, we report here the effect of the $t\bar{t}Z$ axial-vector coupling which brings in the contributions of P-wave resonance states. The P-wave contribution to the total cross section has already been studied [8,9], which only appears as the order-β^2 correction, since the P-wave amplitude is of the order β. In contrast with the charmonium and bottomonium resonances, the large widths of the toponium resonances allow the interference of S-wave and P-wave states for $m_t \gtrsim 100$ GeV. This interference gives a term to the $t\bar{t}$ differential cross section proportional to $\beta\cos\theta$, and hence gives rise to the forward-backward (FB) asymmetry of the cross section at order β. In fact it can be shown that the forward-backward asymmetry increases as well as becoming more sensitive to α_s for larger m_t, since the overlaps of S-wave and P-wave states increase with the rapid growth of top-quark width. This is in contrast with the total cross section, which loses sensitivity to α_s due to the smearing effect by the large top-quark width [3]. The FB asymmetry "measures" the degree of overlap of the S-wave and P-wave resonance states. The key point here is that the top-quark width and the energy differences of the resonance levels have the same order of magnitude for $m_t \gtrsim 150$ GeV.

We present a brief illustration of the effect of the axial-vector coupling to the toponium resonance states in Sec. II. The formulation for including the QCD enhancement effect to the axial-vector coupling near the threshold is given in Sec. III. In Sec. IV, the formulas for the differential cross sections and the FB asymmetry are summarized, and their dependences on the various physical parameters are studied. Concluding remarks together with some discussion are given in Sec. V. There another source which may give rise to the FB asymmetry near threshold is discussed.

II. THE EFFECT OF AXIAL-VECTOR COUPLING

We briefly review the effect of the axial-vector coupling of top quark at the $t\bar{t}$ threshold region. It is emphasized that the large top-quark width allows the interference between S-wave and P-wave resonance states, giving rise to the forward-backward asymmetry even at the threshold region.

If we consider only the electroweak interaction, there are a number of tree diagrams associated with the process $e^+e^- \to bW^+\bar{b}W^-$. Among them only one diagram where $t\bar{t}$ are pair created (Fig. 1) is concerned in this paper, since only this diagram is enhanced in the $t\bar{t}$ threshold region. When the QCD interaction is switched on, this particular diagram is enhanced near threshold due to the formation of toponium resonance states by the binding effect of the QCD interaction.

In the $e^+e^- \to t\bar{t}$ process, the $t\bar{t}$ pair produced via the $t\bar{t}V$ ($V = \gamma, Z$) vector vertex has spin parity $J^P = 1^-$, whereas that produced via the $t\bar{t}Z$ axial-vector vertex has $J^P = 1^+$ in the massless electron limit. Thus, the vector vertex is associated with S- and D-wave resonance states, and the axial-vector vertex with P-wave states.

The axial-vector coupling is suppressed by a power of β near threshold as can be seen from the nonrelativistic form of the coupling

$$\bar{t}\gamma^k\gamma_5 t Z^k \simeq \frac{1}{m_t}\epsilon^{ijk}\chi_1^\dagger\sigma^i\chi_2 p^j Z^k + O(p^2), \tag{1}$$

where χ_1 and χ_2 denote two-component spin wave functions of t and $\bar{t}$, respectively, and $2\mathbf{p}$ is the relative three-momentum between t and $\bar{t}$.

In general, S-wave resonance states and P-wave resonance states have different energy spectra. However, the widths of resonances grow rapidly as m_t increases, and they become so large that S-wave and P-wave resonance states start to interfere for $m_t \gtrsim 100$ GeV.

Let us state it more explicitly. At the lowest order, it is expected that the toponium resonances exhibit the Coulomb level spectrum because the binding effect due to gluon exchanges can be regarded as a Coulombic interaction [1]. Then, the level gaps typically become of the order $\alpha_s^2 m_t \sim 1$ GeV, and the S-wave states and P-wave states are degenerate in this approximation. There will be S-wave states corresponding to the principal quantum number $n = 1, 2, 3, \ldots$, and P-wave states for $n = 2, 3, 4, \ldots$. If we consider the higher order corrections, the QCD potential deviates from the Coulomb potential, and the S-wave states and P-wave states are no longer degenerate, with typical level splitting of the order $\alpha_s^3 m_t \sim 0.1$ GeV.

On the other hand, each resonance state has a width almost twice that of the top quark $\Gamma_t \sim G_F m_t^3/8\sqrt{2}\pi$, which grows rapidly as m_t increases. For instance, $\Gamma_t \simeq 0.1$ GeV for $m_t = 100$ GeV, and $\Gamma_t \simeq 1$ GeV for $m_t = 150$ GeV. If we fix the c.m. energy at the $n = 1$ resonance, where no corresponding P-wave resonance exists, the width and the level gap would become comparable for $m_t \gtrsim 150$ GeV. At $n \geq 2$ resonances, there would be larger interference effects. Thus, we anticipate from the above order estimation that the interference would be significant at $n \geq 2$ resonances even for a light top quark, where the resonance structures are more distinct, and also at the $n = 1$ resonance for a relatively heavy top quark.

The P-wave amplitude being of order β at the threshold, its interference with S-wave resonance states gives rise to the order β correction to the leading S-wave contribution to the cross sections. Since this correction stems from the interference of the vector and axial-vector couplings, it is proportional to $\beta\cos\theta$, or, it gives rise to the FB asymmetry at order β. Meanwhile the effect of axial-vector coupling to the total cross section is of the order β^2, which is beyond our scope [9].

III. NONRELATIVISTIC GREEN'S FUNCTION

In this section we present our formalism to evaluate the $e^+e^- \to t\bar{t} \to bW^+\bar{b}W^-$ amplitude with the top-quark axial-vector coupling at the $t\bar{t}$ threshold region. The method to evaluate the S-wave amplitude is described in Ref. [4] in detail, which we will not present in this paper.

It is well known that a quark pair produced near threshold forms resonance states by exchanging gluons between them a number of times. Diagrammatically, this is seen in the ladder diagram where the gluon is exchanged n times between the pair in that it has the behavior $\sim (\alpha_s/\beta)^n$, and hence is not small even for large n if $\beta \sim \alpha_s$. That is, higher order terms in α_s remain unsuppressed. The singularity that appears at this specific kinematical region is known as "threshold singularity."

Since higher order terms can no longer be neglected, we are led to add the ladder diagrams to infinite orders to determine the $t\bar{t}Z$ axial-vector vertex. Let us denote it as Λ_5^μ. (See Fig. 2.) For this purpose, we follow the steps similar to that given in Ref. [3], which deals with the fairly systematic derivation of the $t\bar{t}V$ vector vertex near $t\bar{t}$ threshold.

The axial-vector vertex Λ_5^μ satisfies the self-consistent equation

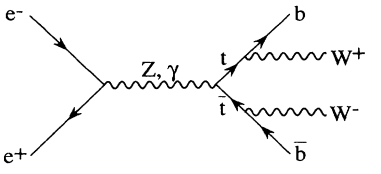

FIG. 1. The diagram which is enhanced near $t\bar{t}$ threshold in the process $e^+e^- \to bW^+\bar{b}W^-$.

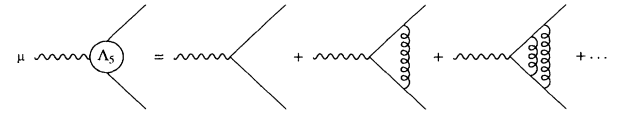

FIG. 2. The diagrams which contain leading threshold singularities to the axial-vector vertex Λ_5^μ. These are the summations of ladder diagrams where any number of uncrossed gluons are exchanged between t and $\bar{t}$.

$$\Lambda_5^\mu(q,p) = \gamma^\mu\gamma_5 + i\int \frac{d^4k}{(2\pi)^4}\,\gamma^\alpha\, S_F(q/2+k)\,\Lambda_5^\mu(q,k) S_F(-q/2+k)\,\gamma_\alpha C_F \frac{4\pi\alpha_s}{(k-p)^2+i\epsilon}, \tag{2}$$

which is depicted diagrammatically in Fig. 3. Here the color factor is given by $C_F = 4/3$, and S_F denotes the top-quark propagator

$$S_F(p) = \frac{i(\not{p}+m_t)}{p^2 - m_t^2 + im_t\Gamma_t}, \tag{3}$$

where Γ_t represents the top-quark on-shell width. Readers are reminded that Eq. (2) shall be sandwiched between propagators $S_F(q/2+p)$ and $S_F(-q/2+p)$, since we are concerned with the process where t and $\bar{t}$ finally decay into bW's. The threshold singularity arises from the loop integral on the right-hand side (RHS) of Eq. (2) when the internal t and $\bar{t}$ momenta are in the nonrelativistic region [10]. Therefore, we will keep only the leading parts as $\beta \to 0$ on both sides of the equation.

For nonrelativistic t and $\bar{t}$, their propagators reduce to the form

$$S_F(q/2+p) \to \left(\frac{1+\gamma^0}{2}\right)\frac{i}{E/2 + p^0 - \mathbf{p}^2/2m_t + i\Gamma_t/2}, \tag{4}$$

$$S_F(-q/2+p) \to \left(\frac{1-\gamma^0}{2}\right)\frac{i}{E/2 - p^0 - \mathbf{p}^2/2m_t + i\Gamma_t/2}, \tag{5}$$

where the Z four-momentum is set as $q = (2m_t + E, \mathbf{0})$ in the $t\bar{t}$ c.m. frame. Meanwhile, the gluon propagator reduces to the instantaneous part as $\beta \to 0$, since it will be sandwiched between the above nonrelativistic t ($\bar{t}$) propagators:

$$\gamma^\alpha \frac{-i}{(k-p)^2+i\epsilon}\gamma_\alpha \to \gamma^0 \frac{i}{|\mathbf{k}-\mathbf{p}|^2}\gamma^0. \tag{6}$$

We may also determine the spinor structure of the vertex $\Lambda_5^\mu(q,p)$ in the nonrelativistic region. As $\Lambda_5^\mu(q,p)$ is contracted with the wave function of virtual Z produced by e^+e^- annihilation, only the space components of $\Lambda_5^\mu(q,p)$ are relevant. Then, if we note that

$$(\not{q}/2 + \not{p} + m_t)\,\gamma^k\gamma_5\,(-\not{q}/2 + \not{p} + m_t) \to -i\,m_t\,(1+\gamma^0)\,\sigma^{kl}\gamma_5 p^l\,(1-\gamma^0) \tag{7}$$

with

$$\sigma^{kl} = \frac{i}{2}\left[\gamma^k, \gamma^l\right], \tag{8}$$

it is expected $\Lambda_5^k(q,p)$ would have the spinor structure

$$\Lambda_5^k(q,p) \simeq (\sigma^{kl}\gamma_5)\left(-\frac{i}{m_t}\right)\Gamma_A^l(q,p) \tag{9}$$

after repeatedly sandwiching (7) by the nonrelativistic propagators (4) and (5), and by $t\bar{t}g$ vertices (6). [See Eq. (1).] Here and hereafter, the Latin indices refer to the space components.

Substituting the above propagators and vertices to Eq. (2), we find

$$\Gamma_A^l(q,p) = p^l - i\int \frac{d^4k}{(2\pi)^4}\,\Gamma_A^l(q,k)\cdot C_F \frac{4\pi\alpha_s}{|\mathbf{k}-\mathbf{p}|^2}\,\frac{1}{E/2 + k^0 - \mathbf{k}^2/2m_t + i\Gamma_t/2}\,\frac{1}{E/2 - k^0 - \mathbf{k}^2/2m_t + i\Gamma_t/2}. \tag{10}$$

The RHS is independent of p^0, so that we may self-consistently set $\Gamma_A^l = \Gamma_A^l(q,\mathbf{k})$ on the RHS, and perform a k^0 integration. Putting

$$\Gamma_A^l(q,\mathbf{p}) = -\tilde{F}^l(\mathbf{p};E)(E - \mathbf{p}^2/m_t + i\Gamma_t), \tag{11}$$

we see that $\tilde{F}^l(\mathbf{p};E)$ becomes the kernel of the nonrelativistic Schrödinger equation:

$$\left[\frac{\mathbf{p}^2}{m_t} - (E+i\Gamma_t)\right]\tilde{F}^l(\mathbf{p};E) = p^l + \int \frac{d^3\mathbf{k}}{(2\pi)^3}\,\tilde{F}^l(\mathbf{k};E)\,C_F\frac{4\pi\alpha_s}{|\mathbf{k}-\mathbf{p}|^2}. \tag{12}$$

Going to the coordinate space, this is equivalent to

$$\left[-\frac{\Delta}{m_t} + V(r) - (E+i\Gamma_t)\right]F^l(\mathbf{x};E) = -i\partial^l\delta^3(\mathbf{x}) \tag{13}$$

with

$$V(r) = -C_F\frac{\alpha_s}{r}. \tag{14}$$

The solution to Eq. (13) can be written formally as

$$F^l(\mathbf{x};E) = i\frac{\partial}{\partial x'^l}\sum_n \frac{\psi_n(\mathbf{x})\psi_n^*(\mathbf{x}')}{E-E_n+i\Gamma_t}\bigg|_{\mathbf{x}'=0}, \tag{15}$$

where $\psi_n(\mathbf{x})$'s are the solutions to the homogeneous Schrödinger equation

$$\left[-\frac{\Delta}{m_t}+V(r)\right]\psi_n = E_n\psi_n. \tag{16}$$

Equation (15) clearly shows that only P-wave states contribute to $F^l(\mathbf{x};E)$, just as we expected in Sec. II.

Thus, we find the axial-vector vertex, when sandwiched between t and $\bar{t}$ propagators near the threshold, is given by

$$S_F(q/2+p)\,\Lambda_5^k(q,p)\,S_F(-q/2+p) \simeq \left(\frac{1+\gamma^0}{2}\sigma^{kl}\gamma_5\frac{1-\gamma^0}{2}\right)\left(-\frac{i}{m_t}\right)\tilde{F}^l(\mathbf{p};E) \times\left(\frac{1}{E/2+p^0-\mathbf{p}^2/2m_t+i\Gamma_t/2}+\frac{1}{E/2-p^0-\mathbf{p}^2/2m_t+i\Gamma_t/2}\right), \tag{17}$$

where $\tilde{F}^l(\mathbf{p};E)$ can be obtained by first solving the Schrödinger equation (13) in the coordinate space to determine $F^l(\mathbf{x};E)$, and then taking its Fourier transform:

$$\tilde{F}^l(\mathbf{p};E) = \int d^3\mathbf{x}\, e^{-i\mathbf{p}\cdot\mathbf{x}}F^l(\mathbf{x};E). \tag{18}$$

At this stage one comment may be in order. Since we have restricted ourselves within the nonrelativistic regime in the loop integration in Eq. (2), one may wonder if the integration over the relativistic regime would give rise to the corrections of the same order of magnitude. It can be shown that the axial-vector vertex $\Lambda_5^k(q,p)$ in general has such a spinor structure that it will be suppressed by β when sandwiched between nearly on-shell t and $\bar{t}$ propagators, just as in Eq. (7). Then, after appropriately renormalizing the ultraviolet divergences, loop integrations over the relativistic regime will further give suppression factors $(\alpha_s)^n$. These in turn are not accompanied by the singularities $\sim(1/\beta)^n$, so that the relativistic corrections are only higher order corrections to (17).

In the remaining part of this section, we give a brief sketch of the method for evaluating the above Green's functions.

Let us first see how to evaluate the Green's function in the coordinate space. It can be shown that the P-wave contribution to $F^l(\mathbf{x};E)$ is given in terms of $f(r)$, the solution to the one-dimensional homogeneous Schrödinger equation, as

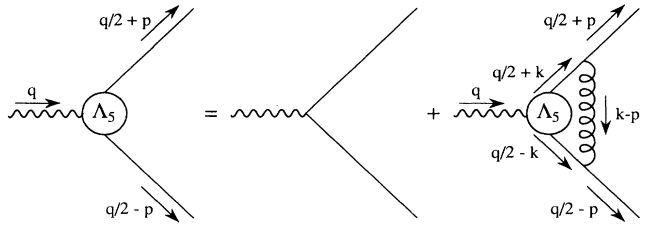

FIG. 3. The self-consistent equation satisfied by the axial-vector vertex $\Lambda_5^\mu(q,p)$.

$$F^l(\mathbf{x};E) = \frac{im_t}{4\pi}\frac{f(r)}{r}\left(\frac{x^l}{r}\right), \tag{19}$$

$$\left[\frac{d^2}{dr^2}+m_t[E+i\Gamma_t-V(r)]-\frac{2}{r^2}\right]f(r)=0, \tag{20}$$

which satisfies the boundary conditions

$$f(r)\to 0 \quad \text{as} \quad r\to\infty, \tag{21}$$

$$f(r)\to\frac{1}{r}+\cdots \quad \text{as} \quad r\to 0. \tag{22}$$

This particular solution $f(r)$ may be obtained as the linear combination of (arbitrary) two independent solutions $f_1(r)$ and $f_2(r)$ to the same homogeneous equation (20). If we write

$$f(r) = A\,[f_1(r)+B\,f_2(r)], \tag{23}$$

the coefficients A and B are readily determined from the boundary conditions (21) and (22) as

$$B = -\lim_{r\to\infty}\frac{f_1(r)}{f_2(r)}, \tag{24}$$

$$A = \left(\lim_{r\to 0} r[f_1(r)+B\,f_2(r)]\right)^{-1}. \tag{25}$$

Thus, $F^l(\mathbf{x};E)$ can be obtained by numerically solving the homogeneous differential equation (20).

The Green's function in the momentum space is expressed as the Fourier integral of $f(r)$. Defining the scalar function $\tilde{F}(\mathbf{p};E)$ by

$$\tilde{F}^l(\mathbf{p};E) = p^l\,\tilde{F}(\mathbf{p};E), \tag{26}$$

we find

$$\tilde{F}(\mathbf{p};E) = \frac{m_t}{p}\int_0^\infty dr\, r f(r)\left(\frac{\sin pr - pr\cos pr}{p^2r^2}\right) \tag{27}$$

with $p=|\mathbf{p}|$.

IV. CROSS SECTIONS

In this section we present the formulas of the differential cross sections for the process $e^+e^-\to t\bar{t}\to bW^+\bar{b}W^-$

including the axial-vector coupling contribution. The axial-vector coupling gives rise to the $t\bar{t}$ distribution proportional to $\cos\theta$, which leads to the forward-backward (FB) asymmetry of the cross section. The FB asymmetry below threshold (at the resonance peak) increases from 0 to $\sim 7\%$ as m_t is raised from 100 GeV to 200 GeV. It also grows as the c.m. energy increases, and exceeds 10% in the continuum region. The Green's functions are evaluated using the two-loop improved QCD potential given in Ref. [4] for $V(r)$ in the Schrödinger equations. The QCD potential incorporates the running of the coupling constant α_s, which is also the inclusion of higher order corrections. We note that all the analyses in this section do not include the effect of the initial-state radiation. We also neglect the bottom-quark mass ($m_b = 0$) for simplicity.

Near $t\bar{t}$ threshold, the leading QCD enhancement is contained in the $t\bar{t}V$ vector vertex in the diagram shown in Fig. 1. According to Refs. [3, 4], we should replace the vector vertex together with t and $\bar{t}$ propagators in the pure electroweak process by

$$S_F(p_t)\,\gamma^k S_F(-\bar{p}_t) \to \left(\frac{\not{p}_t + m_t}{2m_t}\,\gamma^k\,\frac{-\not{\bar{p}}_t + m_t}{2m_t}\right)\left(1 - \frac{8}{3\pi}\alpha_s\right)\tilde{G}(\mathbf{p};E)\;[D(p_t) + D(\bar{p}_t)] \tag{28}$$

in order to incorporate the threshold singularities due to multiple exchanges of gluons between t and $\bar{t}$. Here, t and $\bar{t}$ four-momenta are set as $p_t = (p_t^0, \mathbf{p})$ and $\bar{p}_t = (\bar{p}_t^0, -\mathbf{p})$, respectively, with $p_t^0 + \bar{p}_t^0 = 2m_t + E$ so that E is related to the c.m. energy as $E = \sqrt{s} - 2m_t$. $D(p)$ represents the nonrelativistic top-quark propagator without spinor structure:

$$D(p) = \frac{1}{p^0 - m_t - \mathbf{p}^2/2m_t + i\Gamma_t/2}. \tag{29}$$

The factor $(1 - 8\alpha_s/3\pi)$ takes into account the order α_s correction coming from the loop integration over the relativistic region [11]. This gives formally the same order correction as the axial-vector-coupling contribution. The coupling constant in this factor is evaluated at the top-quark mass scale, $\alpha_s = \alpha_s(m_t)$.

The resonance structure is contained in the S-wave Green's function $\tilde{G}(\mathbf{p};E)$. It is given by the Fourier transform of $G(\mathbf{x};E)$ satisfying the Schrödinger equation in the coordinate space:

$$\left[-\frac{\Delta}{m_t} + V(r) - (E + i\Gamma_t)\right] G(\mathbf{x};E) = \delta^3(\mathbf{x}), \tag{30}$$

$$\tilde{G}(\mathbf{p};E) = \int d^3\mathbf{x}\, e^{-i\mathbf{p}\cdot\mathbf{x}}\, G(\mathbf{x};E). \tag{31}$$

The discussion in the previous section shows that the QCD enhancement effect to the axial-vector vertex can be taken in by a similar replacement:

$$S_F(p_t)\,\gamma^k\gamma_5 S_F(-\bar{p}_t) \to \left(\frac{1+\gamma^0}{2}\,\sigma^{kl}\,\gamma_5\,\frac{1-\gamma^0}{2}\right)\left(-\frac{ip^l}{m_t}\right)\tilde{F}(\mathbf{p};E)\;[D(p_t) + D(\bar{p}_t)], \tag{32}$$

where $\tilde{F}(\mathbf{p};E)$ is given in (27). This gives rise to the order β correction to the leading vector-coupling contribution (28).

We may obtain the differential cross section near threshold using the vector vertex (28) and the axial-vector vertex (32). After integrating the $bW^+\bar{b}W^-$ phase space with the momentum constraint $p_t = p_b + p_{W^+}$ and $\bar{p}_t = p_{\bar{b}} + p_{W^-}$, one finds the momentum distribution of t and $\bar{t}$ as

$$d\sigma = \frac{3\pi^2\alpha^2}{m_t^4}\,\Gamma_t^2\,|D(p_t) + D(\bar{p}_t)|^2\,(T_0 + T_1\cos\theta)(2\pi)^4\delta^4(p_t + \bar{p}_t - q)\,\frac{d^4p_t}{(2\pi)^4}\,\frac{d^4\bar{p}_t}{(2\pi)^4}. \tag{33}$$

Here, θ represents the polar angle of the top-quark three-momentum measured from the electron beam direction. T_0 includes the contributions from S-wave resonance states, whereas T_1 stems from the interference of S-wave and P-wave resonance states:

$$T_0 = \left(1 - \frac{16}{3\pi}\alpha_s\right)\left[\left(-\frac{2}{3} + \chi\, g_V^e g_V^t\right)^2 + \chi^2 (g_A^e)^2 (g_V^t)^2\right]|\tilde{G}(\mathbf{p};E)|^2, \tag{34}$$

$$T_1 = \left(-\frac{2}{3}\,\chi\, g_A^e g_A^t + 2\,\chi^2 g_V^e g_A^e g_V^t g_A^t\right) 2\,\frac{|\mathbf{p}|}{m_t}\,\mathrm{Re}\left[\tilde{G}(\mathbf{p};E)\,\tilde{F}^*(\mathbf{p};E)\right]. \tag{35}$$

The vector and axial-vector couplings associated with e^-e^+Z and $t\bar{t}Z$ vertices are given by

$$g_V^e = -\frac{1}{2} + 2\sin^2\theta_W, \quad g_A^e = \frac{1}{2}, \tag{36}$$

$$g_V^t = \frac{1}{2} - \frac{4}{3}\sin^2\theta_W, \quad g_A^t = -\frac{1}{2}, \tag{37}$$

while the ratio of photon and Z propagators with an appropriate normalization factor is defined as

$$\chi = \frac{1}{4\sin^2\theta_W \cos^2\theta_W} \frac{s}{s-m_Z^2}\bigg|_{s=4m_t^2}. \tag{38}$$

We neglected terms which are suppressed by β^2 in (33).

Furthermore, the time component integration $\int \frac{dp_t^0}{2\pi}\frac{d\bar{p}_t^0}{2\pi}(2\pi)\delta(p_t^0+\bar{p}_t^0-q^0)$ may be performed, and one may obtain the three-momentum distribution of the top quark as

$$\frac{d\sigma}{d|\mathbf{p}|d\cos\theta} = \frac{3\alpha^2\Gamma_t}{2m_t^4}|\mathbf{p}|^2(T_0+T_1\cos\theta). \tag{39}$$

Using the above differential cross section formula, we may calculate the FB asymmetry. However, $\int d|\mathbf{p}|$ integration of T_1 is logarithmically divergent, due to the factor $|\mathbf{p}|/m_t$ in Eq. (35) typical to the P-wave amplitude. In this region, the nonrelativistic approximation breaks down, and higher order terms in β become more and more significant. It has been discussed that higher order corrections would suppress the cross section in the high $|\mathbf{p}|$ region, since available phase space of t and $\bar{t}$ decreases in this domain [4, 12]. We thus restrict the $|\mathbf{p}|$ integration within $|\mathbf{p}|<\Lambda$, where the cutoff Λ is taken as

$$\Lambda^2 = \frac{1}{16m_t^2}(9m_t^2-m_W^2)(m_t^2-m_W^2). \tag{40}$$

For $|\mathbf{p}|>\Lambda$, there would be no allowed kinematical configuration such that either one of t or $\bar{t}$ remains on shell and that the other has an invariant mass larger than m_W^2, simultaneously. The phase space virtually vanishes in this region for $\sqrt{s}\simeq 2m_t$. We therefore define the FB asymmetry as [13]

$$\Delta_{\rm FB} = \frac{1}{\sigma_{\rm tot}}\int_0^\Lambda d|\mathbf{p}|\left[\int_0^1 d\cos\theta - \int_{-1}^0 d\cos\theta\right]\frac{d\sigma}{d|\mathbf{p}|d\cos\theta}. \tag{41}$$

Substituting (39) into the above equation, we find

$$\Delta_{\rm FB} = \int_0^\Lambda d|\mathbf{p}|\,|\mathbf{p}|^2 T_1 \Big/ 2\int_0^\Lambda d|\mathbf{p}|\,|\mathbf{p}|^2 T_0. \tag{42}$$

In the following, we discuss the dependences of the FB asymmetry $\Delta_{\rm FB}$ and the $t\bar{t}$ differential cross sections on the various physical parameters.

The energy dependences of $\Delta_{\rm FB}$ together with the total cross sections are shown in Figs. 4, 5, and 6 for $m_t = 100$, 150, and 200 GeV, respectively. In each figure, three curves correspond to $\alpha_s(m_Z) = 0.10$, 0.12, and 0.14.

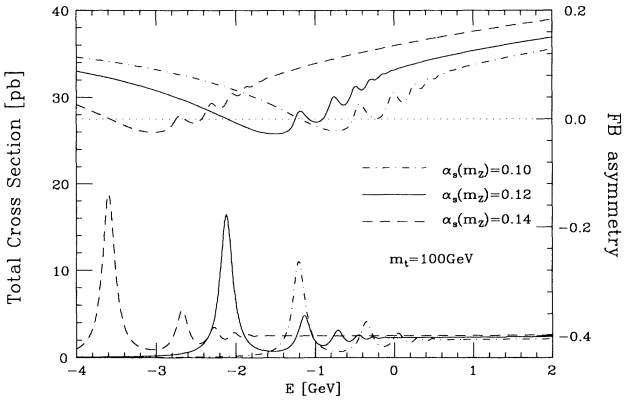

FIG. 4. The total cross section $\sigma(e^+e^-\to t\bar{t})$ and the forward-backward asymmetry $\Delta_{\rm FB}$ vs c.m. energy, taking $m_t = 100$ GeV, for $\alpha_s(m_Z) = 0.10$, 0.12, and 0.14. The energy is measured from twice the top-quark mass: $E = \sqrt{s}-2m_t$. The left axis stands for the total cross section, and the right axis is for the forward-backward asymmetry. The dotted line shows the position of zero for the forward-backward asymmetry.

One sees that the FB asymmetry below threshold (at the peak) almost vanishes for $m_t = 100$ GeV, and increases for larger m_t. This is because the top-quark width Γ_t grows rapidly with m_t so that the overlap of S-wave and P-wave resonance states becomes more significant. In each figure, $\Delta_{\rm FB}$ grows as E increases from the lowest lying resonance. This is because the interference among the resonances becomes more severe in higher energies [1, 8], since the resonance levels appear closer to one another.

A fairly complex energy dependence of $\Delta_{\rm FB}$ for $m_t = 100$ GeV, as well as milder behaviors for $m_t = 150$ GeV and $m_t = 200$ GeV, can be understood if we note the analytic structure of the cross sections in the complex E plane. In Fig. 7, we plot the position of poles of $T_1 \propto {\rm Re}[\tilde{G}(\mathbf{p};E)\tilde{F}^*(\mathbf{p};E)]$ together with $\Delta_{\rm FB}$ for

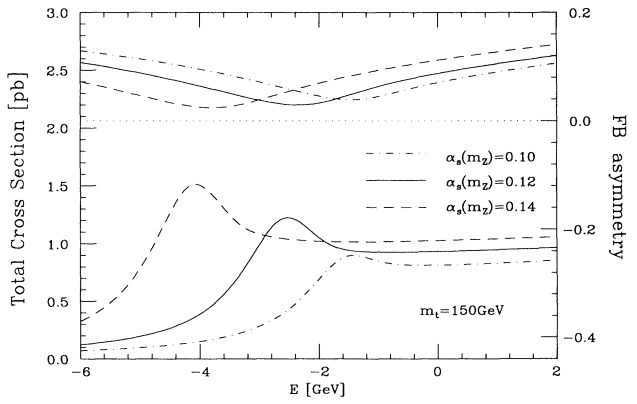

FIG. 5. The total cross section $\sigma(e^+e^-\to t\bar{t})$ and the forward-backward asymmetry $\Delta_{\rm FB}$ vs c.m. energy, with $m_t = 150$ GeV. The notation is the same as in Fig. 4.

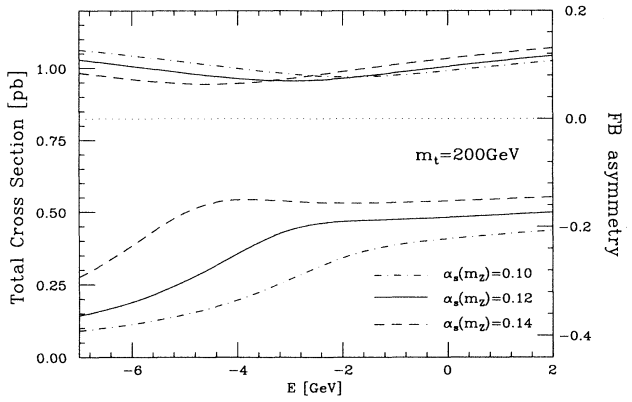

FIG. 6. The total cross section $\sigma(e^+e^- \to t\bar{t})$ and the forward-backward asymmetry $\Delta_{\rm FB}$ vs c.m. energy, with m_t = 200 GeV. The notation is the same as in Fig. 4.

m_t = 100 GeV and $\alpha_s(m_Z)$ = 0.12; see Eqs. (35) and (42). The squares represent the S-wave resonance states ($1S$, $2S$,...), while the crosses represent the P-wave states ($1P$, $2P$,...) [14]. P-wave states lie slightly below the corresponding S-wave states due to the running effect of strong coupling constant. P-wave states "see" the long distance behavior of the QCD potential as compared to S-wave states [15], and thus gain larger binding energies. The dense spectra above threshold ($E > 0$) give quasi-continuum cross sections [8].

Let us increase the energy E along the real axis from below the lowest lying resonance. As E is increased, T_1 changes sign each time E crosses over above the pole. Therefore, $\Delta_{\rm FB}$ oscillates as E is increased. However, when the energy differences of resonance levels become small as compared to Γ_t, many levels begin to contribute, and T_0 tends to be shifted in the positive direction. Indeed, the FB asymmetry at some resonance peak behaves as

$$\Delta_{\rm FB} \propto \left(\frac{\Gamma_t}{\Delta E}\right)^2 \qquad \text{for } \Gamma_t \ll \Delta E, \tag{43}$$

and

$$\Delta_{\rm FB} \propto \sqrt{\frac{\Gamma_t}{m_t}} \qquad \text{for } \Gamma_t \gg \Delta E, \tag{44}$$

where ΔE represents the energy difference of the resonance levels. Equation (43) shows that $\Delta_{\rm FB}$ increases as Γ_t^2 for small m_t. Meanwhile, Eq. (44) implies that asymptotically $\Delta_{\rm FB}$ will grow proportionally to m_t, since $\Gamma_t \propto m_t^3$ for $m_t \gg m_W$ [2].

In Fig. 8, we show the m_t dependence of $\Delta_{\rm FB}$ evaluated at the c.m. energies corresponding to the position of the lowest lying peak that appears in the total cross section. The three curves are for $\alpha_s(m_Z)$=0.10, 0.12, and 0.14. Curves in the dotted lines show that there no longer appear the peaks in the total cross sections for large m_t. In this region, $\Delta_{\rm FB}$ is evaluated at $E = -1.4, -2.5$, and -4.1 GeV for $\alpha_s(m_Z) = 0.10, 0.12$, and 0.14, respectively, which roughly correspond to the energies where $\Delta_{\rm FB}$ is minimal, or, at the "shoulders" of the cross sections. (See Fig. 6.)

One sees that $\Delta_{\rm FB}$ grows from nearly zero to 6–8% as m_t is increased from 100 GeV to 200 GeV. This is because the top-quark width grows rapidly in this m_t region (Γ_t=0.095 GeV for m_t=100 GeV, and Γ_t=2.5 GeV for m_t=200 GeV), so that the S-wave state and the P-wave state start to overlap, which gives rise to the inter-

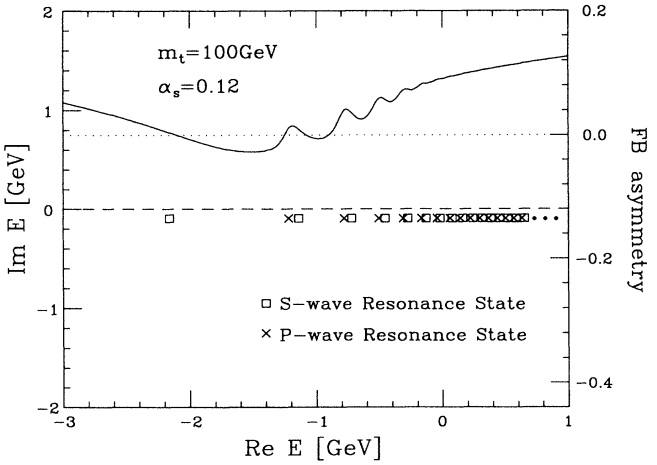

FIG. 7. The positions of poles of T_1 in the complex energy plane, together with the forward-backward asymmetry as a function of energy, taking m_t = 100 GeV and $\alpha_s(m_Z)$ = 0.12. The boxes represent S-wave resonances, and the crosses represent P-wave resonances. The energy is measured from twice the top-quark mass: $E = \sqrt{s} - 2m_t$. The right axis is for the forward-backward asymmetry.

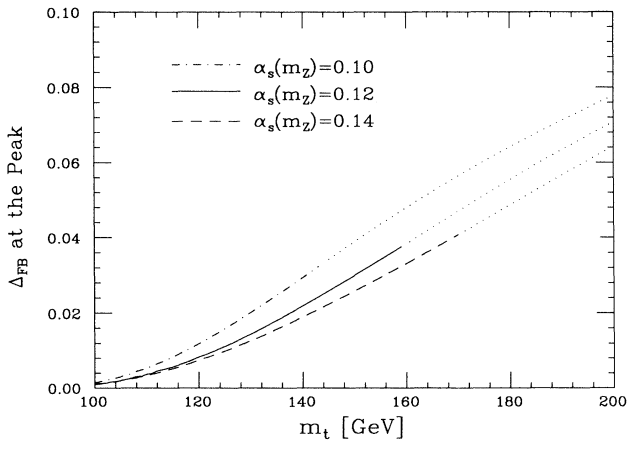

FIG. 8. The forward-backward asymmetry $\Delta_{\rm FB}$, evaluated at the first peak of total cross section, vs top-quark mass, for $\alpha_s(m_Z)$ = 0.10, 0.12, and 0.14. The dotted curves show that there no longer appear the peaks in the cross section for large m_t. In this region, $\Delta_{\rm FB}$ is evaluated at $E = -1.4, -2.5$, and -4.1 GeV, respectively, for $\alpha_s(m_Z)$ = 0.10, 0.12, and 0.14.

ference term proportional to $\cos\theta$ in Eq. (33). Therefore, Δ_{FB} is enhanced for larger m_t, and is more feasible to be measured in experiments, while the total cross section decreases like $\sim 1/m_t^2$, as well as the peak cross section decreasing due to the large top-quark width.

The FB asymmetry at the peak is also dependent on $\alpha_s(m_Z)$: Δ_{FB} decreases as α_s increases. This is because the resonance levels spread apart from one another for larger α_s, and thus the overlap of the S-wave and P-wave states decreases. Although cross sections are more enhanced for larger α_s, the enhancements tend to cancel in the denominator and numerator for the FB asym-

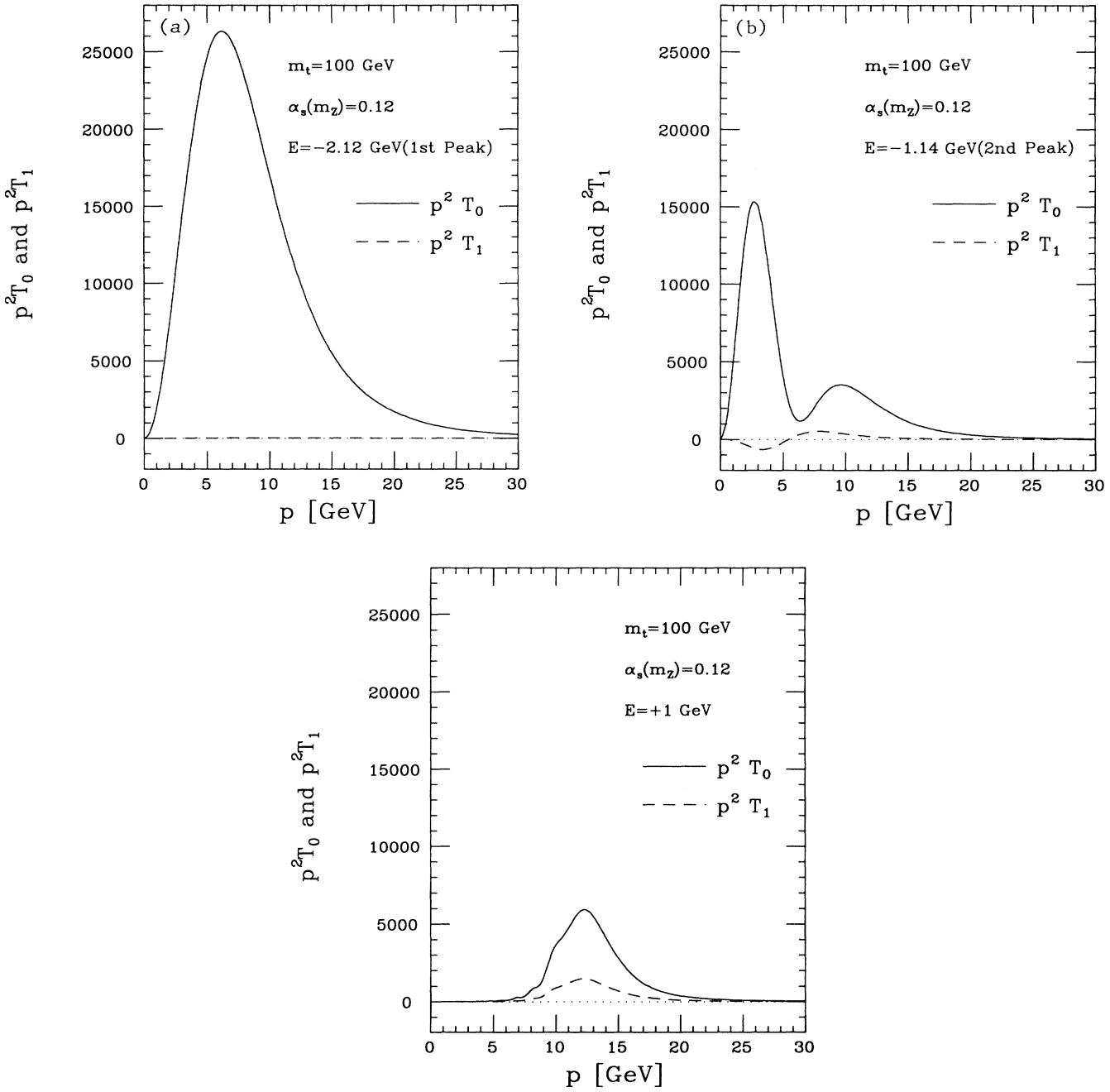

FIG. 9. The comparison of the coefficients of the $t\bar{t}$ differential cross section as a function of top-quark momentum $|\mathbf{p}|$, with $m_t = 100$ GeV and $\alpha_s(m_Z) = 0.12$. The solid curve shows the coefficient for the spherical distribution ($|\mathbf{p}|^2 T_0$), and the dashed curve for the $\cos\theta$ distribution ($|\mathbf{p}|^2 T_1$). The dotted line shows the position of zero. In each figure, the energy ($E = \sqrt{s} - 2m_t$) is taken as (a) $E = -2.12$ GeV (at the first resonance peak), (b) $E = -1.14$ GeV (at the second resonance peak), and (c) $E = +1$ GeV (above threshold).

metry (41). The noticeable feature here is that the α_s dependence of Δ_{FB} is magnified for a heavier top quark. [According to Eq. (44), Δ_{FB} would become independent of α_s asymptotically as $m_t \to \infty$. Nevertheless one sees that the sensitivity to α_s remains for $m_t \lesssim 200$ GeV.]

We are also concerned with the $t\bar{t}$ distributions, which can be investigated by using the differential cross section formulas given by (33) and (39). $t\bar{t}$ distribution is spherical in the leading order, since only S-wave states contribute. The inclusion of axial-vector coupling gives rise to the $\cos\theta$ term at order β. We show in Fig. 9 the $|\mathbf{p}|$ dependences of $|\mathbf{p}|^2 T_0$ and $|\mathbf{p}|^2 T_1$ for $m_t = 100$ GeV. Three figures correspond to the energies (a) at the first peak ($E = -2.12$ GeV), (b) at the

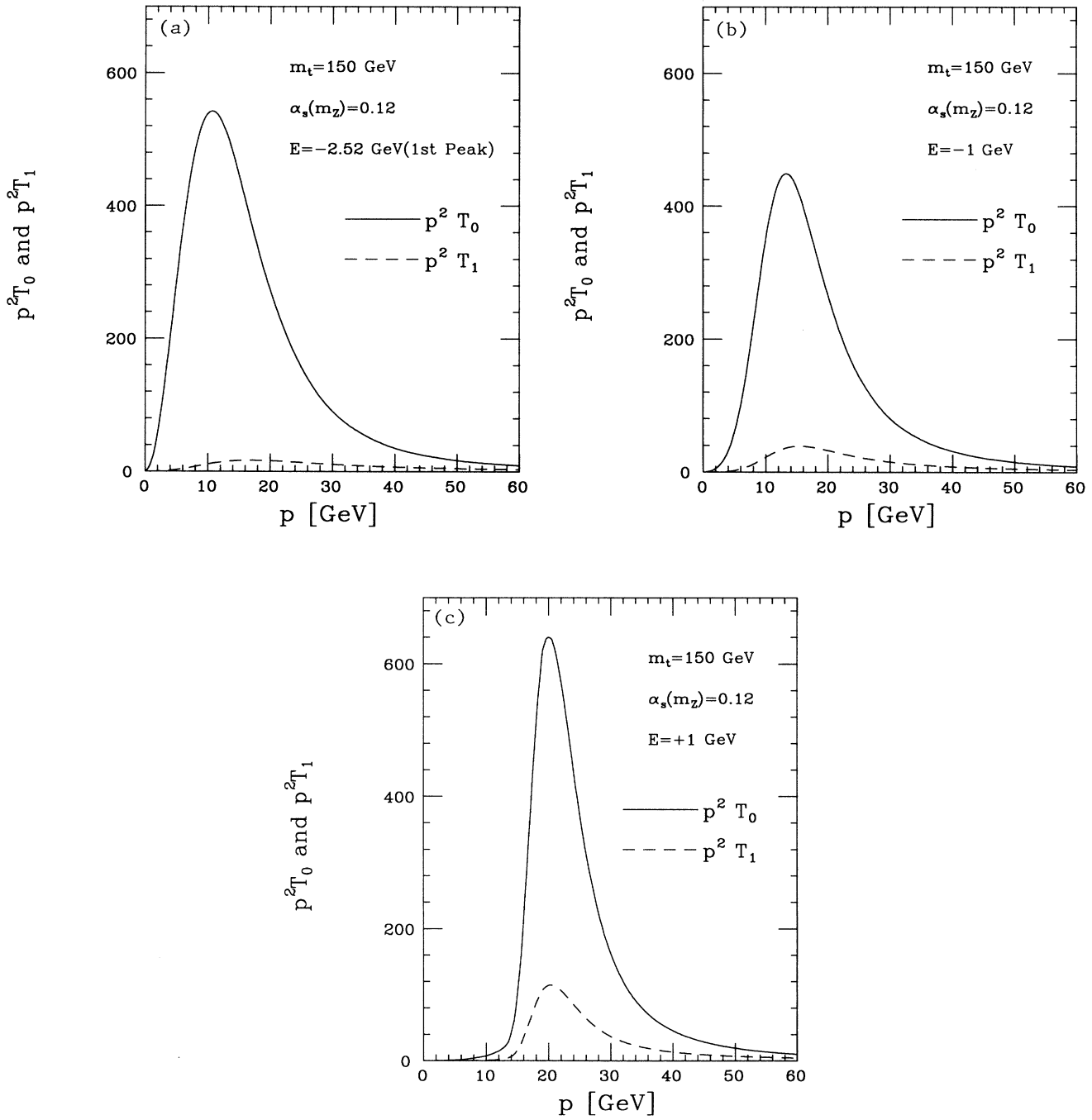

FIG. 10. The comparison of the coefficients of the $t\bar{t}$ differential cross section as a function of top-quark momentum $|\mathbf{p}|$, with $m_t = 150$ GeV and $\alpha_s(m_Z) = 0.12$. Notations are the same as in Fig. 9. The energy ($E = \sqrt{s} - 2m_t$) is taken as (a) $E = -2.52$ GeV (at the peak), (b) $E = -1$ GeV, and (c) $E = +1$ GeV.

second peak ($E = -1.14$ GeV), and (c) above threshold ($E = 1$ GeV). At $E = -2.12$ GeV, T_1 almost vanishes. T_0 exhibits the shape of the absolute square of the $1S$ resonance state wave function in the momentum space. At $E = -1.14$ GeV, T_0 shows the square of the $2S$ state wave function, while T_1 shows the product of the $2S$ state wave function and the $2P$ state wave function. At $E = 1$ GeV, where a number of resonance states contribute, the structure of the $t\bar{t}$ distribution is quite smeared, and T_1 is more enhanced. The peak of the distribution is shifted to higher $|\mathbf{p}|$ compared to $E = -2.12$ GeV and $E = -1.14$ GeV, since the kinetic energy of $t(\bar{t})$ is larger.

Similarly, the $|\mathbf{p}|$ dependences of $|\mathbf{p}|^2 T_0$ and $|\mathbf{p}|^2 T_1$ for $m_t = 150$ GeV are shown in Fig. 10, at the enregies (a) $E = -2.52$ GeV (first peak), (b) $E = -1$ GeV, and (c) $E = 1$ GeV. The structures of the $t\bar{t}$ distributions are smeared out compared to those of $m_t = 100$ GeV due to the larger top-quark width.

Thus, Figs. 9 and 10 show that the effect of axial-vector coupling modifies the $t\bar{t}$ distribution significantly for large m_t, and at the higher c.m. energies.

In summary, the FB asymmetry below threshold (at the lowest lying peak of the total cross section for $m_t \lesssim 150$ GeV) "measures" the degree of overlap of S-wave states and P-wave states. It is essentially determined by the relative magnitude of the widths and the energy differences of the resonance levels, while it is insensitive to the normalization of the cross sections. This suggests that $\Delta_{\rm FB}$ would be a stable quantity to the smearing effect by the initial-state radiation. Quite generally, $\Delta_{\rm FB}$ increases as the resonance widths increase or the binding energy decreases, provided that the FB asymmetry stems solely from the interference of S-wave and P-wave states. The FB asymmetry is more enhanced for larger m_t. In particular, its dependence on α_s is magnified for 150 GeV $\lesssim m_t \lesssim$ 200 GeV. This sensitivity may help the determination of α_s for a relatively heavy top quark, since much of the resonance structures are smeared out in the total cross section.

V. CONCLUSION AND DISCUSSION

We have investigated the axial-vector-coupling contribution to the $t\bar{t}$ pair production cross section near the threshold. This contribution is a part of the order-β corrections to the $e^+e^- \to t\bar{t} \to bW^+\bar{b}W^-$ process. The large top-quark width allows the interference between S-wave resonance states produced by the vector coupling and P-wave states produced by axial-vector coupling, giving rise to the FB asymmetry already at the threshold. As m_t is varied from 100 GeV to 200 GeV, the FB asymmetry at the resonance peak increases from 0% to $\sim 7\%$, allowing its experimental study. We also studied the α_s dependence of the asymmetry. A careful study of the FB asymmetry at future e^+e^- colliders allows an efficient cross-check to the measurement of α_s, which will be done by the total cross section and bW invariant-mass distribution [4].

We may address the possible role of the FB asymmetry for a relatively heavy top quark ($m_t \gtrsim 150$ GeV) as follows. The main defect in the measurement of the threshold total cross section for a heavy top quark is that the resonance structures are quite smeared, and that it is difficult to tell whether m_t is small or α_s is large. One of the candidates to resolve such correlation in the measurement of α_s and m_t is to measure the differential cross sections at the threshold [4]. Here, we demonstrated that the FB asymmetry measured at the first peak (or, at the shoulder) of the total cross section may be used in measuring α_s. In spite of the smearing of the resonance structures, there still exist the resonance poles in the amplitude. It is seen that the FB asymmetry can measure the level splittings, while it is insensitive to the normalization of the cross sections. Since the level structure is among the basic quantities of QCD in the threshold region, it is worth emphasizing that a part of the structure is measurable even with the large resonance widths.

We have made a cross-check on our results by comparing them to the tree-level FB asymmetry calculated in the continuum region. We evaluated the FB asymmetry with the Coulomb potential for the small coupling constant $\alpha_s = 0.01$, which approximates the tree-level calculation with a small enhancement near threshold. The FB asymmetry with the realistic potential is larger. These features match well with those that are expected from the analysis on the total cross sections in Ref. [8]. We have also checked that our analysis is insensitive to the long-range part of the QCD potential. We varied the long-range linear rising behavior of the potential, and confirmed that the effect on the FB asymmetry is insignificant. This confirms the original observation by Fadin and Khoze [1].

Although our results should be enough to convince the readers that the top-quark threshold physics is rich in phenomenology, some cautions should be made on the analysis presented in this paper.

Here, we studied the FB asymmetry due to the interference between S-wave and P-wave resonance states. However, there is another type of higher order correction which may become the source of FB asymmetry near threshold at order β. It is found that the one-soft-gluon exchange between t and $\bar{b}$ ($\bar{t}$ and b), and between b and $\bar{b}$, would give rise to the order-β correction to the threshold cross sections, where b and $\bar{b}$ are the decay products of $t\bar{t}$ pair produced via $t\bar{t}V$ vector coupling. (See Fig. 11.) Because the decay $t \to bW$ occurs via the V-A inter-

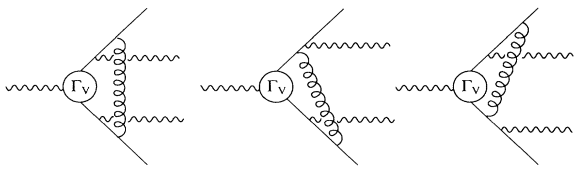

FIG. 11. The diagrams which also contribute to the order-β corrections to the leading threshold singularities. These involve one-soft-gluon exchange between t and $\bar{b}$ ($\bar{t}$ and b), and between b and $\bar{b}$.

action, it may also contribute to the FB asymmetry after exchanging gluons. However, these corrections come purely from the $t\bar{t}V$ vector coupling, and hence contributions come only from the S- and D-wave states. Thus, they can be treated independently from our results on the interference between S- and P-wave resonance states. A full study including all the order-β (= order-α_s) corrections requires the summation over all diagrams contributing at the order α_s^{n+1}/β^n. Such a study is now underway [7]. Thus, the study we presented in this paper should be regarded as an intermediate report.

It should be noted that the FB asymmetry is already an order-β quantity, always of the order 10%, and there will be order-β^2 corrections which will appear as a theoretical uncertainty of the order 1%. This uncertainty persists even after studying the full order-β corrections, and requires some of the order-β^2 calculations in order to establish the reliable theoretical prediction of the FB asymmetry. We believe such calculations will be attained in due time.

To study the physics sensitivity at the future e^+e^- colliders, we also have to take the initial-state radiation as well as the bremsstrahlung effects into account. However, we expect that their effects on the FB asymmetry will be small. For a relatively light top quark $m_t \sim 100$ GeV, the resonance peaks appear quite distinct. In this case, the FB asymmetry on the second peak will not suffer smearing due to the contributions of other higher level peaks, since they have much lower peak heights and are far apart from the second peak. For a relatively heavy top quark $m_t \gtrsim 150$ GeV, the FB asymmetry is a smooth function of the energy, and integration over the electron luminosity functions will not give large deviations from the integrands.

ACKNOWLEDGMENTS

We express special gratitude to S. Ishihara, whose help has been essential to complete this work. We are also grateful to K. Hikasa, K. Hagiwara, K. Fujii, C.-K. Ng, and the members of the JLC Working Group for fruitful discussions.

[1] V.S. Fadin and V.A. Khoze, Pis'ma Zh. Eksp. Teor. Fiz. **46**, 417 (1987) [JETP Lett. **46**, 525 (1987)]; Yad. Fiz. **48**, 487 [Sov. J. Nucl. Phys. **48**, 309 (1988)].
[2] K. Fujikawa, Prog. Theor. Phys. **61**, 1186 (1979).
[3] M. Strassler and M. Peskin, Phys. Rev. D **43**, 1500 (1991).
[4] Y. Sumino, K. Fujii, K. Hagiwara, H. Murayama, and C.-K. Ng, Phys. Rev. D (to be published).
[5] J. Schwinger, *Particles, Sources, and Fields* (Addison-Wesley, New York, 1973), Vol. 2, Chap. 5-4.
[6] T. Appelquist and H. Politzer, Phys. Rev. Lett. **34**, 43 (1975); Phys. Rev. D **12**, 1404 (1975).
[7] K. Hikasa and Y. Sumino (unpublished).
[8] W. Kwong, Phys. Rev. D **43**, 1488 (1991).
[9] V.S. Fadin and V.A. Khoze, Yad. Fiz. **53**, 1118 (1991) [Sov. J. Nucl. Phys. **53**, 692 (1991)].
[10] See, for example, M. Braun, Zh. Eksp. Teor. Fiz. **54**, 1220 (1968) [Sov. Phys. JETP **27**, 652 (1968)].
[11] R. Barbieri, R. Gatto, R. Kögerler, and Z. Kunszt, Phys. Lett. **57B**, 455 (1975); W. Buchmüller, and S.-H.H. Tye, Phys. Rev. D **24**, 132 (1981); see also Ref. [8].
[12] I.I. Bigi, V.S. Fadin, and V. Khoze, Nucl. Phys. **B377**, 461 (1992).
[13] Since the integration over $|\mathbf{p}|$ is only logarithmically dependent on the cutoff Λ, our choice of the cutoff should be safe.
[14] We follow the convention for lighter quarkonium resonances in naming the P-wave states. This differs, however, from the principal quantum number for the Coulomb levels; see Sec. II.
[15] This "long distance" is still much shorter than the infrared QCD region $\sim \Lambda_{\rm QCD}^{-1}$. See Figs. 9 and 10.